*Mapana – Journal of Sciences*
2025, Vol. 24, No. 1, 79-96
ISSN 0975-3303 | https://doi.org/10.12723/mjs.72.6

# A Theoretical Study of Coumarin Derivatives: Exploring DSSC, NLO Properties and Pharmacokinetics

Subhani Khanam Nehal*, Renuka U*, Mahanthesh M Basanagouda† Suresh Kumar H M‡ and Thipperudrappa J*

## Abstract

This study presents a comprehensive theoretical analysis of the coumarin derivatives 1-(4-Methoxy-phenoxymethyl)-benzo[f] chromen-3-one (4MPBCO) and 6-Methoxy-4-(4-methoxy-phenoxymethyl)-chromen-2-one (6M4MPC) using density functional theory (DFT). The various molecular properties of these molecules are explored through the examination of geometrical parameters, frontier molecular orbitals (FMO), molecular electrostatic potential (MEP) maps and natural bonding orbitals (NBO). The HOMO-LUMO energies were calculated to assess the suitability of these molecules for dye-sensitized solar cell (DSSC) applications. In addition, the non-linear optical (NLO) parameters were evaluated to determine their potential for NLO applications. Furthermore, the physicochemical and ADMET properties were computed to examine the molecule's suitability for pharmacokinetic applications.

**Keywords:** Coumarin derivatives, DFT, NLO, NBO, ADMET.

## 1. Introduction

Coumarin and its derivatives are widely found in plants and foods, where they serve critical roles as bacteriostats, fungistats and growth regulators[1,2]. Known for their utility as laser dyes in the blue-green spectrum, coumarins have broad applications in numerous scientific and technological fields[3]. Their strong UV-visible fluorescence properties make them excellent candidates for use as colouring agents [4] and non-

* Department of Studies in Physics, Vijayanagara Sri Krishnadeveraya University, Ballari – 583105, Karnataka, India; subhanikhanamnehal@gmail.com; jtrphy2007@gmail.com
† P.G. Department of Chemistry, P.C. Jabin Science College, Hubli - 580031, Karnataka, India; mahanteshachem@gmail.com
‡ Department of Physics, Siddaganga Institute of Technology, Tumakuru-572103, Karnataka, India; sureshkumarhm@gmail.com

linear optical chromophores[5]. Beyond their industrial and technological uses, coumarins exhibit a range of therapeutic activities, including anti-inflammatory, antioxidant, antitumor, antidiabetic, antimicrobial and anti-neurodegenerative effects[6-11]. These compounds are also notable for their pharmacokinetic and pharmacological attributes, enhancing their suitability for chemosensing applications[12]. In the medical context, coumarins are employed as optical brighteners, fluorescent indicators, anticoagulants, sunscreens and agents in the treatment of HIV, cancer and tuberculosis[13-17].

The extensive applicability of the fundamental coumarin molecule and its derivatives across various fields has generated significant interest in exploring the properties and potential applications of new coumarin derivatives. Among these 1-(4-Methoxy-phenoxymethyl)-benzo[f]chromen-3-one (4MPBCO) and 6-Methoxy-4-(4-methoxy-phenoxymethyl)-chromen-2-one (6M4MPC) have been identified as promising candidates. Introducing additional functional groups to the coumarin skeleton can significantly alter its chemical, biological and electronic properties. For example, substituting a methoxy group on the coumarin skeleton has been shown to enhance its biological activity[18]. With this motivation, investigations have been carried out to elucidate the geometry, electronic properties, chemical reactivity, bonding interactions, optical characteristics and drug-like attributes of the 4MPBCO and 6M4MPC molecules, which have largely remained unexplored in the existing literature.

In this research, we have explored various properties of 4MPBCO and 6M4MPC, using bond length and bond angles and focusing on their electronic characteristics, including the energies of the highest occupied molecular orbital (HOMO), lowest unoccupied molecular orbital (LUMO) and the energy gap. These analyses provide important insights into the chemical reactivity of these derivatives. We have also calculated global reactivity parameters and generated molecular electrostatic potential (MEP) maps to support our findings. Furthermore, we conducted natural bonding orbitals (NBO) analysis to quantify intermolecular bonding interactions. Understanding the non-linear optical (NLO) properties of 4MPBCO and 6M4MPC by using hyperpolarizability and polarizability to evaluate their potential applications in non-linear optical devices. Additionally, we assessed their drug-like properties, given their promising bio-applications. Through this comprehensive investigation, we aim to explore new applications and enhance our understanding of these novel compounds.

## 2. Materials and methods

### 2.1. Materials

The coumarin derivatives, namely 1-(4-Methoxy-phenoxymethyl)-benzo[f] chromen-3-one (4MPBCO) and 6-Methoxy-4-(4-methoxy-phenoxymethyl)-

chromen-2-one (6M4MPC), were synthesised by our research team[19] and utilised in the present study without any additional purification. The molecular structures of 4MPBCO and 6M4MPC are depicted in Figure 1.

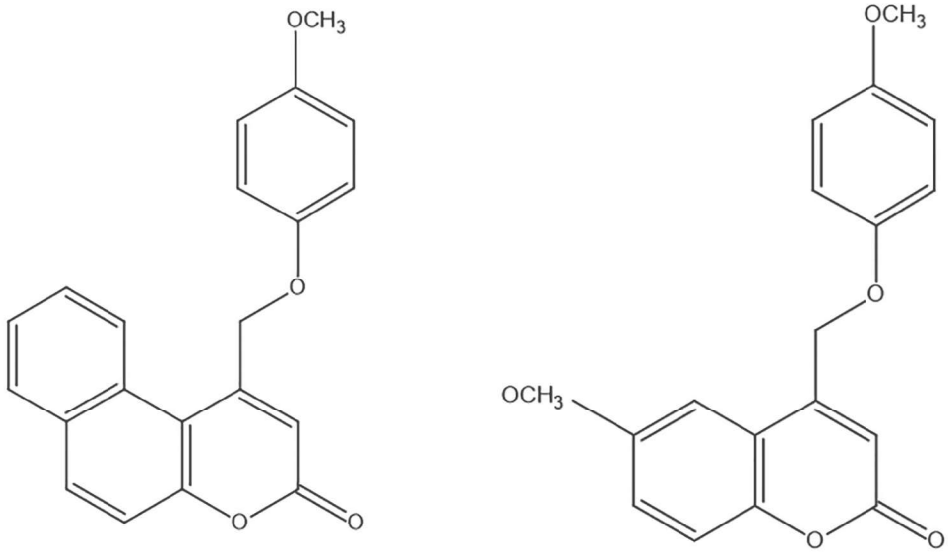


(a) 4MPBCO (b) 6M4MPC

**Figure 1:** (a) Molecular structure of 4MPBCO and (b)6M4MPC

## 2.2. Methods

### 2.2.1. Computational Methods

Quantum chemical calculations for 4MPBCO and 6M4MPC were conducted using Gaussian 09 software[20], and visualisation was performed using GaussView 6.0[21]. The optimised parameters of the 4MPBCO and 6M4MPC molecules were computed employing density functional theory (DFT) at the B3LYP level with a 6-311G basis set, incorporating polarisation (p,d) and diffuse (++) functions. The B3LYP method was chosen for its ability to accurately describe medium-sized molecules while maintaining computational efficiency[22]. Natural Bonding Orbital (NBO) analysis was performed using NBO version 3.1 integrated into Gaussian 09[23], and nonlinear optical properties were studied using Multiwfn software[24]. Drug likeness properties of 4MPBCO and 6M4MPC were evaluated using online tools such as SwissADME[25] and Molinspiration[26].

## 3. Results and Discussion

### 3.1 Optimized structure of titled molecules

The structures of 4MPBCO and 6M4MPC were optimised using the DFT/B3LYP/6-311G++(d,p) method in the gas phase. Figure (2) illustrates

the optimised geometries of 4MPBCO and 6M4MPC, along with their corresponding dipole vectors. The optimisation results indicate that both 4MPBCO and 6M4MPC exhibit C1 point group symmetry, making them completely asymmetric in structure[27]. The computed ground-state dipole moments are 5.90 Debye and 5.63 Debye, respectively, indicating the polar nature of these molecules.

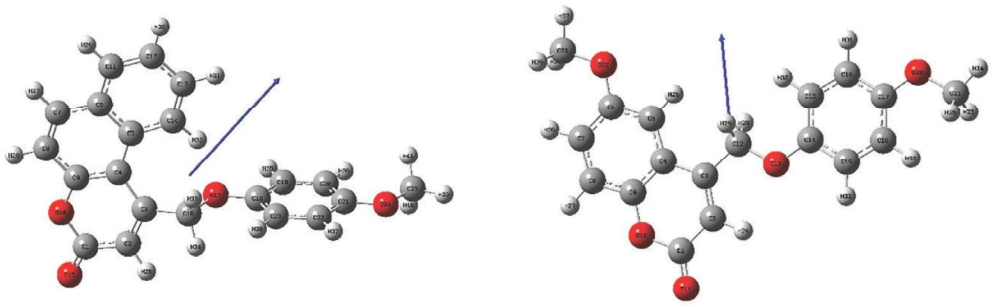

a) 4MPBCO b) 6M4MPC

**Figure 2:** (a) Optimized structure of 4MPBCO and (b) Optimized structure of 6M4MPC with dipole vector.

## 3.2 Geometrical parameters of optimised structure of titled molecules

To understand the molecular geometry of the titled molecules, their optimised structures were used. The geometrical parameters, such as bond lengths and bond angles for both 4MPBCO and 6M4MPC, are provided in Supplementary Table S1. To gain a deeper understanding of these geometrical parameters, a Mulliken charge distribution analysis was performed, providing a clear depiction of the charges associated with each atom, as shown in Supplementary Figure S1. Generally, homonuclear bond lengths are longer than heteronuclear bond lengths due to the repulsion between like charges and the attraction between opposite charges[28].

According to the principle of attraction and repulsion between like and unlike charged atoms, the geometrical parameters exhibit variations in certain bond lengths and bond angles[29]. After optimisation, both molecules show the highest C-C bond length of 1.51 Å. This is due to opposite charges on C3-C16 in 4MPBCO and C3-C12 in 6M4MPC. Both molecules contain additional C-C bonds measuring 1.46 Å in length. The presence of double bond character significantly influences bond length, with increased charge sharing in C-C double bonds leading to compression. In 4MPBCO, the three C-C double bonds have lengths ranging from 1.36 Å to 1.38 Å, while in 6M4MPC, a single C-C double bond measures 1.35 Å. Notably, the computed C-C double bonds are shorter in length compared to single C-C bonds. The C16-O17(1.43 Å) bond length in 4MPBCO has the highest length compared

to other C-O bonds because it connects coumarin with methoxy benzene. In 6M4MPC, the O22-C23 and O20-C21 bond lengths are the longest at 1.43 Å, attributed to the presence of like charges, which causes bond elongation. The C-H bond lengths in both molecules range from 1.08 Å to 1.10 Å.

The bond angles also adhere to the principle of attraction and repulsion[29]. In 4MPBCO, the bond angle between C3-C4-C5 is the largest at 127°. This increase is due to all three carbons carrying the same charge, which leads to repulsion and a widening of the angle. In contrast, 6M4MPC features the largest bond angle at C2-C1-O10, measuring 116°. Here, C2 and O10 are negatively charged, while C1 is positively charged, resulting in a greater angle. Furthermore, the electronegative oxygen atom attracts charge towards itself, contributing to the larger angle in this molecule. All the computed theoretical data is in good agreement with the experimental XRD data of the similar molecule[19].

## 3.3 Electronic and chemical reactivity parameters

### 3.3.1. HOMO-LUMO and Energy Gap

Frontier molecular orbital (FMO) analysis provides insights into the charge transfer properties of molecules, which in turn could influence their bioactive nature[30]. This analysis yields the examination of the HOMO and LUMO energy levels, and also sheds light on the chemical reactivity of the molecules. The Frontier molecular orbitals of the coumarin derivatives 4MPBCO and 6M4MPC were computed using the DFT/6-311++G(d,p) level to understand the chemical reactivity of the molecules. Converting the computed energy values from Hartree to electron volts (eV) is achieved using the conversion factor i.e. 1Hartree = 27.211 eV. Figure (3) illustrates the HOMO-LUMO orbitals of 4MPBCO and 6M4MPC molecules, where red colour represents the positive phase and green colour indicates the negative phase. In Figure (3), the charge density for both 4MPBCO and 6M4MPC are primarily concentrated around the methoxy-phenoxymethyl group in the HOMO level. At the LUMO level, the charge density is primarily localised on the coumarin group in both molecules, with additional localisation on the phenyl group attached to the coumarin skeleton in the 4MPBCO molecule. This suggests that both molecules indicate a strong tendency for intramolecular charge transfer from the methoxy-phenoxymethyl group to the coumarin core. Furthermore, the computed HOMO energy value of both molecules is -5.99 eV which is lower than the potential of redox electrolyte (-4.9 eV), satisfying one of the conditions for DSSC applications [31]. In the same way, the computed LUMO energy values of titled molecules are -2.45 eV (4MPBCO) and -2.18 eV (6M4MPC). These values are considerably higher than the $TiO_2$ conduction band energy level (-4.0 eV), satisfying another requirement for DSSC applications[31]. Further, these HOMO-LUMO energy values

are comparable to literature values[32] on Benzothiazole-based coumarin derivatives, which are proposed to be better DSSC materials. The HOMO-LUMO energies are used to calculate the energy gap of these molecules, which are found to be 3.54 eV (4MPBCO) and 3.81 eV (6M4MPC). Again, the energy gap of both molecules is compared with existing literature [32] on Benzothiazole-based coumarin derivatives. The energy gap values of both the molecules are outside the range of reported values (2.21 to 3.13 eV). This limits the application of these molecules for DSSC applications. However, these materials satisfy two important conditions for DSSC applications, hinting at the possible use of these molecules for DSSC applications after tuning their energy gap by judiciously adding suitable functional groups.

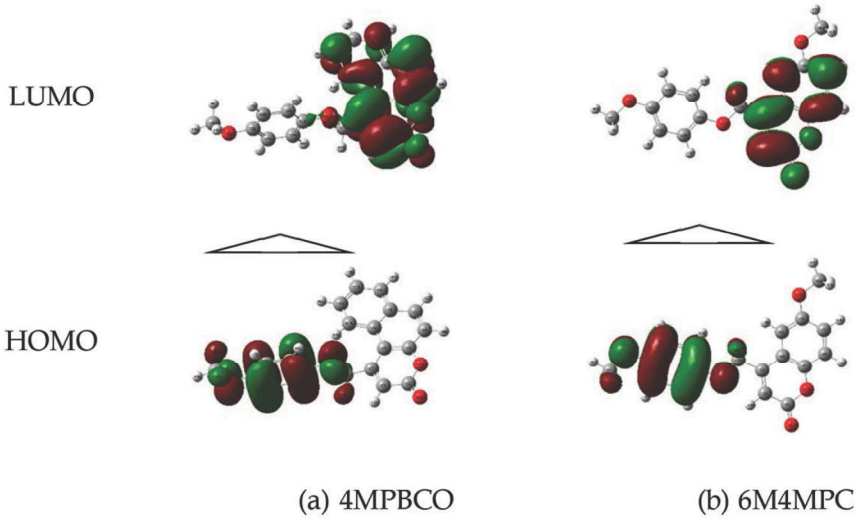


**Figure 3:** 3D representation of the HOMO-LUMO electron energy distribution of (a) 4MPBCO (b) 6M4MPC molecules.

### 3.3.2. Chemical Reactivity

The HOMO-LUMO energy values are utilised to calculate several chemical reactivity parameters, including ionisation potential (IP), electron affinity (EA), chemical potential (μ), hardness (η), softness (S), electrophilicity (ω) and electronegativity ($\chi$) using Koopman's formula[33]. These calculated values are listed in Table 1.

**Table 1:** Reactivity descriptors of 4MPBCO and 6M4MPC

| Molecule | $E_{HOMO}$ (eV) | $E_{LUMO}$ (eV) | $E_G$ (eV) | $I_P$ (eV) | $E_A$ (eV) | μ (eV) | η (eV) | □ ($eV^{-1}$) | $\chi$ (eV) | ω (eV) |
|---|---|---|---|---|---|---|---|---|---|---|
| 4MPBCO | -5.99 | -2.45 | 3.54 | 5.99 | 2.45 | -4.22 | 1.77 | 0.56 | 4.22 | 5.03 |
| 6M4MPC | -5.99 | -2.18 | 3.81 | 5.99 | 2.18 | -4.08 | 1.91 | 0.52 | 4.08 | 4.36 |

The energy required to remove an electron from the Highest occupied molecular orbitals is termed ionisation potential[34] and was found to be 5.99 eV for both molecules because, in both molecules, HOMO is localised over the methoxy benzene group. Electron affinity is the tendency of a molecule to accept an electron[35]. The electron affinity of 4MPBCO is higher than that of 6M4MPC due to the presence of a weakly electron-withdrawing phenyl group on the sixth position of the coumarin core of 4MPBCO, which enhances the electron affinity. In contrast, in 6M4MPC, the methoxy group occupies the same position as the phenyl group in 4MPBCO but functions as an electron-donating group, increasing electron density and subsequently lowering its electron affinity. Chemical potential (μ) measures the potential energy of the molecules to exchange with their surroundings[36]. A more negative chemical potential indicates a stronger tendency for particles to leave the substance. Therefore, 4MPBCO, with its lower chemical potential of -4.22 eV compared to 6M4MPC's -4.08 eV, suggests 4MPBCO has a higher electron concentration or a greater tendency to emit electrons than 6M4MPC. Hardness quantifies a molecule's resistance to undergo electronic transitions[37], with 6M4MPC(1.91 eV) being slightly harder than 4MPBCO(1.77 eV) respectively. While softness gauges its propensity for transitions[38], with 6M4MPC (0.52 eV) being slightly more compliant than 4MPBCO (0.56 eV). Electronegativity reflects the tendency of an atom to attract electrons in a chemical bond and is the negative of the chemical potential[39]. For 4MPBCO, the electronegativity is 4.22 eV, while for 6M4MPC, it is 4.08 eV. This indicates that 4MPBCO has a higher electron-attracting ability in chemical bonds compared to 6M4MPC. The electrophilicity index (ω) measures a molecule's reactivity towards electron-rich species[40]. 4MPBCO has a higher index (5.03 eV) compared to 6M4MPC (4.36 eV), indicating 4MPBCO's greater propensity to react with nucleophiles or electron-donating species. Overall, the results indicate that 4MPBCO is more chemically active than 6M4MPC.

To gain a thorough insight into the reactive zones within the 4MPBCO and 6M4MPC molecules, a Molecular Electrostatic Potential (MEP) study is conducted. MEP is a valuable tool for identifying electrophilic and nucleophilic regions, which are crucial for biological recognition processes and hydrogen bonding interactions[36]. It employs a colour gradient to depict the strength of charge distribution, with red indicating electron-rich regions (electrophilic sites) and blue indicating electron-deficient regions (nucleophilic sites) [41]. Figure 4 shows an MEP map of both molecules, highlighting that the electrophilic sites are primarily around the electronegative oxygen atoms. The nucleophilic sites are located on the methoxy group and, to a lesser extent, on the benzene ring of the coumarin molecule. The green regions represent the neutral areas in both molecules.

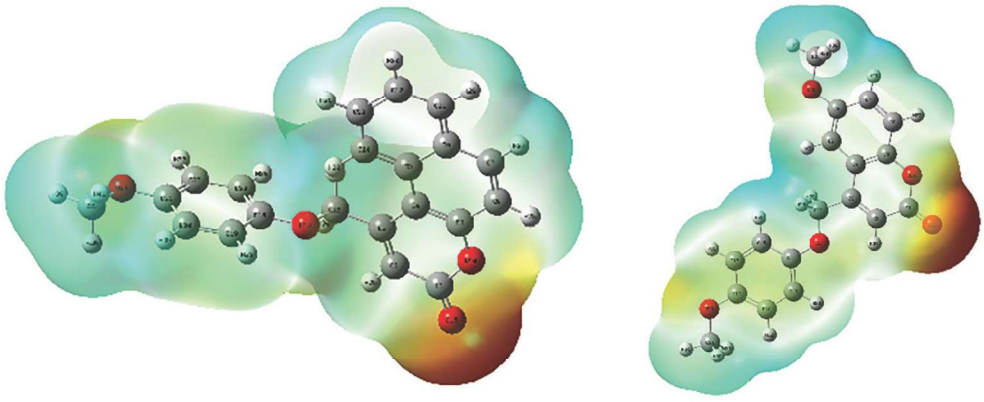

a) 4MPBCO b) 6M4MPC

**Figure 4:** 3D representation of the MEP map of (a)4MPBCO and (b) 6M4MPC molecules.

### 3.4 Natural Bonding Orbitals (NBO) analysis of the titled molecules.

The second-order Fock matrix was utilised to investigate the donor-acceptor interactions within the molecule in the NBO analysis. NBO analysis was performed on both 4MPBCO and 6M4MPC molecules at the B3LYP/6-311++G(d,p) level to study intramolecular interactions, rehybridisation and electron density delocalisation within the molecule[42]. The energy $E(2)$ associated with each donor (i) to an acceptor (j) delocalisation is determined using the second-order perturbation method using equation 1.

$$E(2) = \Delta E_{ij} = q_i \frac{F(i,j)^2}{\varepsilon_i - \varepsilon_j} \quad \text{..... (1)}$$

where $q_i$ is the donor orbital occupancy $\varepsilon_i$ and $\varepsilon_j$ are diagonal elements and $F(i,j)^2$ off-diagonal NBO Fock matrix elements [42]. A higher $E(2)$ value indicates a more intense molecular interaction between electron donors and acceptors, signifying greater conjugation within the molecular system. The delocalisation of electron density between occupied Lewis-type (bond or lone pair) NBO orbitals and unoccupied (antibond or Rydberg) non-Lewis NBO orbitals corresponds to a stabilising donor-acceptor interaction[43].

The computed NBO parameters specifically bond type, occupancy and stabilisation energy E(2) values, are presented in Table 2. The bond type provides insight into the nature of the chemical bonds, occupancy indicates the electron distribution in molecular orbitals, and the E(2) value represents the strength of interactions within the molecule. According to Table 2, the NBO analysis for the 4MPBCO molecule revealed a stable $\pi^* - \sigma^*$ interaction, with the highest interaction energy observed from the donor C20-C21 to the acceptor C18-C19 in the methoxybenzene ring at 12,560 kcal/mol. In contrast, for the 6M4MPC molecule, the highest interaction energy was

observed in a σ to σ* interaction from the donor C12-H29 to the acceptor C21-H34 within the molecule at 10,817 kcal/mol. These results emphasise the importance of the lone pairs on the electronegative oxygen atom, which remain localised and do not participate in bonding while interacting with nearby carbon atoms.

**Table 2a:** Selected second-order perturbation theory analysis of Fock matrix in NBO basis of 4MPBCO molecule.

| Donor | Bond Type | Occupancy | Acceptor | Bond Type | Occupancy | E(2) (kcal/mol) |
|---|---|---|---|---|---|---|
| C20 - C21 | π* | 0.407 | C18 - C19 | σ* | 0.022 | 12560 |
| C20 - C21 | π* | 0.407 | C25 - H41 | σ* | 0.020 | 2595 |
| C20 - C21 | π* | 0.407 | C25 - H40 | σ* | 0.019 | 868 |
| C20 - C21 | π* | 0.407 | C21 - O24 | σ* | 0.030 | 151 |
| C5 - C6 | π* | 0.460 | C3 - C16 | σ* | 0.024 | 131 |
| C20 - C21 | π* | 0.407 | C3 - C16 | σ* | 0.024 | 114 |
| C13 - C14 | π* | 0.265 | C3 - C16 | σ* | 0.024 | 92 |
| C22 - C23 | π* | 0.369 | C18 - C23 | σ* | 0.029 | 73 |
| O15 | LP(2) | 1.831 | C1 - O10 | σ* | 0.127 | 39 |
| O24 | LP(1) | 1.963 | C3 - C16 | σ* | 0.024 | 35 |
| C19 - C20 | σ | 1.972 | C3 - C16 | σ* | 0.024 | 21 |
| O17 | LP(1) | 1.965 | C18 - C23 | σ* | 0.029 | 8 |
| O10 | LP(1) | 1.963 | C4 - C9 | σ* | 0.031 | 7 |
| C 1 - C2 | σ | 1.982 | C3 - C16 | σ* | 0.024 | 6 |
| C 2 - C3 | π | 1.805 | C16 - O17 | σ* | 0.029 | 6 |
| C22 - H37 | σ | 1.977 | C3 - C16 | σ* | 0.024 | 6 |
| C18 - C19 | π | 0.392 | C21 - O24 | σ* | 0.030 | 6 |
| C 4 - C9 | σ | 1.971 | C3 - C16 | σ* | 0.024 | 5 |
| C16 - O17 | σ | 1.986 | O17 - C18 | σ* | 0.032 | 5 |

**Table 2b :** Selected second-order perturbation theory analysis of Fock matrix in NBO basis of 6M4MPC molecule.

| Donor | Bond Type | Occupancy | Acceptor | Bond Type | Occupancy | E(2) (kcal/mol) |
|---|---|---|---|---|---|---|
| C12 - H29 | σ | 1.970 | C21 - H34 | σ* | 0.009 | 10817 |
| C23 - H38 | σ | 1.995 | C21 - H34 | σ* | 0.009 | 2668 |
| O10 | LP(1) | 1.963 | C21 - H34 | σ* | 0.009 | 2517 |
| C1 - O11 | π | 1.979 | C21 - H34 | σ* | 0.009 | 2130 |
| O13 | LP(1) | 1.963 | C23 - H37 | σ* | 0.009 | 2008 |
| C23 - H37 | σ | 1.991 | C21 - H34 | σ* | 0.009 | 1837 |
| O22 | LP(1) | 1.963 | C21 - H34 | σ* | 0.009 | 1748 |
| C23 - H39 | σ | 1.995 | C23 - H37 | σ* | 0.009 | 1444 |

| | | | | | | |
|---|---|---|---|---|---|---|
| C2 - C3 | σ | 1.976 | C21 - H34 | σ* | 0.009 | 975 |
| C15 - C16 | π* | 0.371 | C21 - H34 | σ* | 0.009 | 400 |
| C17 - C18 | π* | 0.407 | C23 - H37 | σ* | 0.009 | 329 |
| C14 - C19 | π | 1.652 | C23 - H37 | σ* | 0.009 | 134 |
| C4 - C9 | π* | 1.600 | C23 - H37 | σ* | 0.009 | 93 |
| C6 - O22 | σ | 1.992 | C21 - H34 | σ* | 0.009 | 92 |
| C17 - O20 | σ | 1.992 | C21 - H34 | σ* | 0.009 | 87 |
| C7 - H26 | σ | 1.977 | C17 - O20 | σ* | 0.030 | 13 |
| C2 - H24 | σ | 1.973 | C3 - C4 | σ* | 0.030 | 6 |
| C21 - H34 | σ | 1.991 | C17 - O20 | σ* | 0.030 | 5 |
| C15 - C16 | σ | 1.972 | O13 - C14 | σ* | 0.030 | 5 |

### 3.5 Non-linear Optical (NLO) property of titled molecules.

NLO properties were performed on both 4MPBCO and 6M4MPC molecules at the B3LYP/6-311++G(d,p) level of theory. The nonlinear optical properties of organic molecules are applied in various optical and sensing applications due to their unique characteristics. Multiwfn software was employed to determine the polarizability and hyperpolarizability values of both molecules, which are listed in Table 3. Polarizability offers valuable insights into the molecule's electronic distribution, which is essential for understanding its optical and electronic properties. Additionally, the HOMO-LUMO gap derived from FMO studies suggests greater polarizability enhances charge transfer[44]. On the other hand, first-order hyperpolarizability influences the movement of electron clouds within π conjugated frameworks. The computed values of NLO are presented in Table 3. The hyperpolarizability values for 4MPBCO and 6M4MPC molecules exceed that of urea ($\beta_0$=0.34×10$^{-30}$ e.s.u) by more than 6 and 7.9 times, respectively, indicating their potential for NLO-based applications[45]. The calculated greater polarizability of both molecules also indicates their bioactive nature[46]. The experimental validation of the NLO properties of the titled molecules using the z-scan technique could be used to confirm their potential for NLO applications, which is planned in our future work.

**Table 3:** The polarizability and hyperpolarizability values of 4MPBCO and 6M4MPC

| Molecule | Dipole moment (debye) | Polarizability (e.s.u) | Hyperpolarizability (e.s.u) |
|---|---|---|---|
| 4MPBCO | 5.90 | $4.08 \times 10^{-23}$ | $2.03 \times 10^{-30}$ |
| 6M4MPC | 5.63 | $3.57 \times 10^{-23}$ | $2.69 \times 10^{-30}$ |

### 3.6 Physicochemical and ADMET parameter calculations of tilted molecules

The physicochemical and ADMET (absorption, distribution, metabolism, excretion, and toxicity) characteristics of both 4MPBCO and 6M4MPC molecules were investigated to assess their suitability for pharmacokinetic

applications. Using online tools, namely SwissADME and Molinspiration, the parameters used to describe the physicochemical and ADMET behaviour of the titled molecules are listed in Table 4. From Table 4, both these molecules follow the Lipinski rule of five, indicating their potential to be orally active drugs in humans[47].

**Table 4:** ADMET parameters of 4MPBCO and 6M4MPC molecules

| Molecule | 4MPBCO | 6M4MPC | Acceptable Range | Acceptability (Yes/No) |
|---|---|---|---|---|
| Molecular weight | 332.35 | 312.32 | < 500 Da | Yes |
| WLog P (Lipophilicity) | 3.24 | 4.38 | $\leq 5$ | Yes |
| TPSA | 48.67 | 57.9 | < 140 | Yes |
| H-bond acceptors | 4 | 5 | $\leq 10$ | Yes |
| H-bond donors | 0 | 0 | $\leq 5$ | Yes |

Further, to visualise the physicochemical properties of molecules, particularly their ability to permeate cell membranes for human intestinal absorption (HIA) and cross the blood-brain barrier (BBB), the BOILED-Egg model has been used. The BOILED-Egg model uses the WLOGP (lipophilicity) versus TPSA (polar surface area) plot, and it classifies the molecules into three regions based on their gastrointestinal (GI) absorption and blood-brain barrier (BBB) permeability. The presence of a molecule in the yolk (yellow region) represents the molecule's ability to cross the BBB, indicating potential Central Nervous System (CNS) activity. The presence of a molecule in egg white (white region) represents the molecule's ability to be well-absorbed in the GI tract but not BBB-permeable. The presence of a molecule outside the egg (grey region) represents the molecule's low GI absorption and poor BBB permeability, suggesting limited oral bioavailability and CNS penetration [48]. The BOILED-EGG plots for **4MPBCO** and **6M4MPC** are shown in Figure 5. From the figure, it is observed that both **4MPBCO** and **6M4MPC molecules** are located in the **yellow region** of the BOILED-EGG plot, indicating their **high ability for blood-brain barrier (BBB) penetration.** For a molecule to exist in the **yellow region**, it must have low polarity (TPSA<75) and moderate lipophilicity (WLOGP between 0.4 and 6), which enables the effective BBB penetration [49]. From Table 4 it is observed that TPSA and WLOGP values of both the molecules are satisfying these conditions and are effective for BBB penetration.

Another tool that is crucial in drug discovery and medicinal chemistry is the oral bioavailability chart, which highlights the six key factors essential for drug formulation. The six essential molecular properties are defined as LIPO (lipophilicity), INSOLU (solubility), SIZE (molecular weight), POLAR (polarity) , FLEX (flexibility), and INSATU (saturation)[50]. Lipophilicity determines the drug's ability to permeate lipid membranes. Solubility ensures the drug remains sufficiently dissolved in gastrointestinal fluids for absorption. Molecular size indicates that the drug is small enough to pass

through cellular membranes. Polarity maintains an optimal balance between hydrophilic and lipophilic properties, aiding absorption. Flexibility allows the drug to adopt favourable conformations for interaction with biological membranes and proteins, and Saturation gives the fraction of carbons in the sp3 hybridisation [50][51]. The pink region in the bioavailability chart indicates physicochemical space for bioavailability, and the red line indicates oral bioavailability properties. The oral bioavailability chart for 4MPBCO and 6M4MPC molecules is presented in Figure 5. From Figure 5, it is observed that five parameters out of six fall within the acceptable range for both molecules, whereas the saturation parameter slightly exceeds the acceptable range. This indicates that further optimisation studies are essential to improve the molecule's overall pharmacokinetic profile.

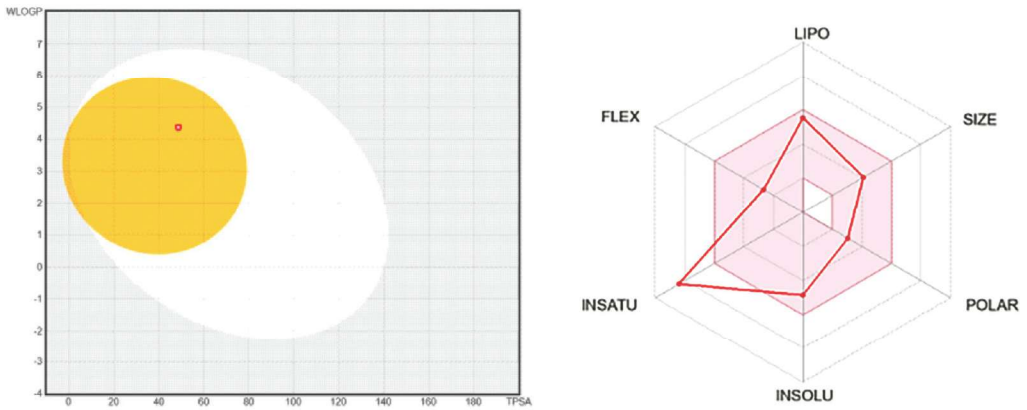


(I) (II)

**Figure 5(a):** (I)Predicted BOILED-Egg plot and (II)Bioavailability radar chart for 4MPBCO molecule

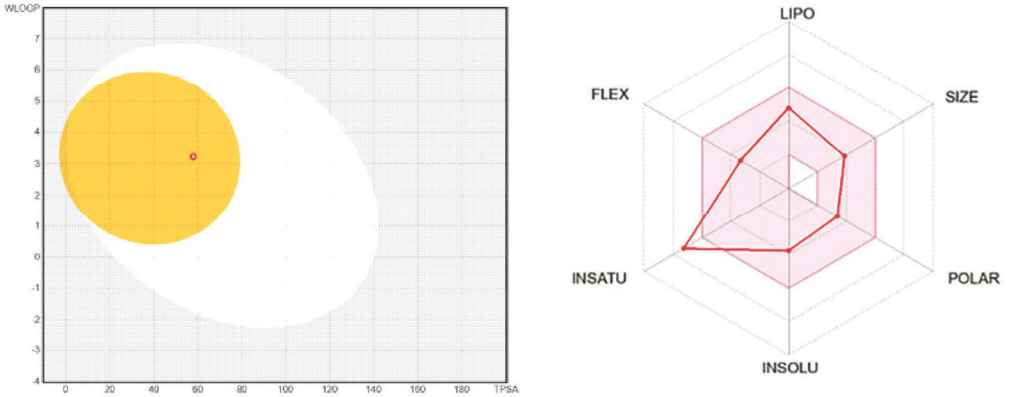


(I) (II)

**Figure 5(b):** (I)Predicted BOILED-Egg plot and (II) Bioavailability radar chart for 6M4MPC molecule

## Conclusion

The computed geometrical parameters of 4MPBCO and 6M4MPC molecules have shown good agreement with XRD data from the literature. The analysis of charge distribution in HOMO and LUMO energy levels of both the titled molecules suggests the intra-molecular charge transfer. The smaller value of the HOMO-LUMO energy gap indicates the high chemical reactivity of both molecules. These materials satisfy two important conditions for DSSC applications, hinting at their possible use in DSSC applications after tuning their energy gap by judiciously incorporating suitable functional groups. MEP analysis highlights the presence of the electrophilic sites primarily around the electronegative oxygen atoms and nucleophilic sites located on the methoxy group and, to a lesser extent, on the phenyl group of the coumarin molecule. The higher value of first-order hyperpolarizability of both the molecules by more than 6 and 7.9 times, respectively, compared to urea, hints that both the molecules are suitable for NLO applications. Furthermore, NBO analysis indicates more intense $\pi^*$- $\sigma^*$ and $\sigma$-$\sigma^*$ bond interactions for 4MPBCO and 6M4MPC molecules, respectively. The physicochemical and ADMET properties demonstrate favourable results that are suitable for the pharmacokinetics of these molecules. The investigated molecule's application in stated areas requires experimental validation, which is planned in our future work.

## Conflict of Interest:

We, the authors of this manuscript, declare that there is no conflict of interest concerning this work.

## Author Contribution

**Subhani Khanam Nehal:** Investigation, Visualization, Data curation, Formal Analysis, Writing- Original draft preparation, **Renuka U:** Investigation, Data curation, Formal Analysis, **Mahanthesh M Basanagouda:** Resources, **Suresh Kumar H M:** Data curation, Visualization, Resources, **Thipperudrappa J:** Conceptualization, Methodology, Supervision, Writing – review & editing.

## Acknowledgement

First author greatly acknowledges the Department of Minorities, Government of Karnataka for providing the Ph.D. Fellowship to conduct the PhD research work.

## References


[1]. Nagaraja, D., Melavanki, R. M., Patil, N. R., Kusanur, R. A., Thipperudrappa, J., & Sanningannavar, F. M. (2013). Quenching of the excitation energy of coumarin dyes by aniline. *Canadian Journal of Physics*, *91*(11), 976-980. https://doi.org/10.1139/cjp-2013-0009

[2]. Emus-Medina, A., Contreras-Angulo, L. A., Ambriz-Perez, D. L., Vazquez-Olivo, G., & Heredia, J. B. (2023). UV light stress induces phenolic compounds in plants. In *Plant phenolics in abiotic stress management* (pp. 415-440). Singapore: Springer Nature Singapore. https://doi.org/10.1007/978-981-19-6426-8_19

[3]. Mannekutla, J. R., Mulimani, B. G., & Inamdar, S. R. (2008). Solvent effect on absorption and fluorescence spectra of coumarin laser dyes: evaluation of ground and excited state dipole moments. *Spectrochimica Acta Part A: Molecular and Biomolecular Spectroscopy*, *69*(2), 419-426. https://doi.org/10.1016/j.saa.2007.04.016

[4]. Pramod, A. G., Nadaf, Y. F., & Renuka, C. G. (2019). Synthesis, photophysical, quantum chemical investigation, linear and non-linear optical properties of coumarin derivative: Optoelectronic and optical limiting application. *Spectrochimica Acta Part A: Molecular and Biomolecular Spectroscopy*, *223*, 117288. https://doi.org/10.1016/j.saa.2019.117288

[5]. Bansal, Y., Sethi, P., & Bansal, G. (2013). Coumarin: a potential nucleus for anti-inflammatory molecules. *Medicinal Chemistry Research*, *22*, 3049-3060.

[6]. Kostova, I., Bhatia, S., Grigorov, P., Balkansky, S., S Parmar, V., K Prasad, A., & Saso, L. (2011). Coumarins as antioxidants. *Current medicinal chemistry*, *18*(25), 3929-3951.https://doi.org/10.2174/092986711803414395

[7]. Wu, Y., Xu, J., Liu, Y., Zeng, Y., & Wu, G. (2020). A review on anti-tumor mechanisms of coumarins. *Frontiers in oncology*, *10*, 592853.https://doi.org/10.3389/fonc.2020.592853

[8]. Li, H., Yao, Y., & Li, L. (2017). Coumarins as potential antidiabetic agents. *Journal of Pharmacy and Pharmacology*, *69*(10), 1253-1264.https://doi.org/10.1111/jphp.12774

[9]. Smyth, T., Ramachandran, V. N., & Smyth, W. F. (2009). A study of the antimicrobial activity of selected naturally occurring and synthetic coumarins. *International journal of antimicrobial agents*, *33*(5), 421-426.https://doi.org/10.1016/j.ijantimicag.2008.10.022

[10]. Flores-Morales, V., Villasana-Ruíz, A. P., Garza-Veloz, I., González-Delgado, S., & Martinez-Fierro, M. L. (2023). Therapeutic effects of coumarins with different substitution patterns. *Molecules*, *28*(5), 2413.https://doi.org/10.3390/molecules28052413

[11]. Balewski, Ł., Szulta, S., Jalińska, A., &Kornicka, A. (2021). A mini-review: Recent advances in coumarin-metal complexes with biological properties. *Frontiers in Chemistry*, *9*, 781779.https://doi.org/10.3389/fchem.2021.781779

[12]. Zhang, G., Zheng, H., Guo, M., Du, L., Liu, G., & Wang, P. (2016). Synthesis of polymeric fluorescent brightener based on coumarin and its performances on paper as light stabilizer, fluorescent brightener and surface sizing agent. *Applied Surface Science*, *367*, 167-173.https://doi.org/10.1016/j.apsusc.2016.01.110

[13]. Katerinopoulos, H. E. (2004). The coumarin moiety as chromophore of fluorescent ion indicators in biological systems. *Current pharmaceutical design*, *10*(30), 3835-3852.https://doi.org/10.2174/1381612043382666

[14]. Arora, R. B., & Mathur, C. N. (1963). Relationship between structure and anti-coagulant activity of coumarin derivatives. *British journal of pharmacology and chemotherapy*, *20*(1), 29-35.https://doi.org/10.1111/j.1476-5381.1963.tb01294.x

[15]. Kasperkiewicz, K., Erkiert-Polguj, A., & Budzisz, E. (2016). Sunscreening and photosensitizing properties of coumarins and their derivatives. *Letters in Drug Design & Discovery*, *13*(5), 465-474.

[16]. Xu, Z., Chen, Q., Zhang, Y., & Liang, C. (2021). Coumarin-based derivatives with potential anti-HIV activity. *Fitoterapia*, *150*, 104863.https://doi.org/10.1016/j.fitote.2021.104863

[17]. Emami, S., &Dadashpour, S. (2015). Current developments of coumarin-based anti-cancer agents in medicinal chemistry. *European Journal of Medicinal Chemistry*, *102*, 611-630.https://doi.org/10.1016/j.ejmech.2015.08.033

[18]. Shkoor, M., Thotathil, V., Al-Zoubi, R. M., Su, H. L., & Bani-Yaseen, A. D. (2023). Combined experimental and computational investigations of the fluorosolvatochromism of chromeno [4, 3-b] pyridine derivatives: Effect of the methoxy substitution. *Spectrochimica Acta Part A: Molecular and Biomolecular Spectroscopy*, *303*, 123210.https://doi.org/10.1016/j.saa.2023.123210

[19]. Gowda, R., Gowda, K. A., Basanagouda, M., & Kulkarni, M. V. (2011). 6-Chloro-4-(4-methylphenoxymethyl)-2H-chromen-2-one. Acta Crystallographica Section E: Structure Reports Online, 67(7), o1650-o1650. https://doi.org/10.1107% 2FS1600536811019258

[20]. Frisch, A. (2009). gaussian 09W Reference. Wallingford, USA, 25p, 470.

[21]. Dennington, R., Keith, T., & Millam, J. (2009). GaussView, version 5.

[22]. Liu, Y., Zhao, J., Li, F., & Chen, Z. (2013). Appropriate description of intermolecular interactions in the methane hydrates: an assessment of DFT methods. Journal of computational chemistry, 34(2), 121-131. https://doi.org/10.1002/jcc.23112

[23]. Glendening, E. D., Badenhoop, J. K., Reed, A. E., Carpenter, J. E., Bohmann, J. A., Morales, C. M., & Weinhold, F. (1998). University of Wisconsin. Madison, NBO Version, 3. https://doi.org/10.1515/9783110660074

[24]. Lu, T., & Chen, F. (2012). Multiwfn: A multifunctional wavefunction analyzer. Journal of computational chemistry, 33(5), 580-592. https://doi.org/10.1002/jcc.22885].

[25]. Jomroz, M. H. (2004). 'Vibrational Energy distribution Analysis VEDA4 (Warsaw)Daina, A., Michielin, O., & Zoete, V. (2017). SwissADME: a free web tool to evaluate pharmacokinetics, drug-likeness and medicinal chemistry friendliness of small molecules. Scientific reports, 7(1), 42717. https://doi.org/10.1038/srep42717

[26]. Mani, S., Swargiary, G., Gulati, S., Gupta, S., & Jindal, D. (2023). Molecular docking and ADMET studies to predict the anti-breast cancer effect of aloin by targeting estrogen and progesterone receptors. Materials Today: Proceedings, 80, 2378-2384. https://doi.org/10.1016/j.matpr.2021.06.362]

[27]. Tsukerblat, B. S. (2006). Group theory in chemistry and spectroscopy: a simple guide to advanced usage. Courier Corporation.

[28]. Raja, M., Muhamed, R. R., Muthu, S., & Suresh, M. (2017). Synthesis, spectroscopic (FT-IR, FT-Raman, NMR, UV–Visible), NLO, NBO, HOMO-LUMO, Fukui function and molecular docking study of (E)-1-(5-bromo-2-hydroxybenzylidene) semicarbazide. Journal of Molecular Structure, 1141, 284-298. https://doi.org/ 10.1016/j.molstruc.2017.03.117

[29]. Lanke, S. K., & Sekar, N. (2016). Coumarin push-pull NLOphores with red emission: solvatochromic and theoretical approach. Journal of fluorescence, 26, 949-962. https://doi.org/10.1007/s10895-016-1783-6

[30]. Khalid, M., Ullah, M. A., Adeel, M., Khan, M. U., Tahir, M. N., & Braga, A. A. C. (2019). Synthesis, crystal structure analysis, spectral IR, UV–Vis, NMR assessments, electronic and nonlinear optical properties of potent quinoline based derivatives: Interplay of experimental and DFT study. Journal of Saudi Chemical Society, 23(5), 546-560. https://doi.org/10.1016/j.jscs.2018.09.006

[31]. Renuka, U., Subhani Khanam Nehal, N. M. Mallikarjuna, K. Vibha, S. M. Kumar, H. M. Kumar, and Thipperudrappa Javuku. "Computational and Spectroscopic Study of Newly Synthesized Bio-Active Azo Dyes: DFT, Solvatochromism, and Preferential Solvation." CHEMISTRYSELECT 9, no. 48 (2024).

[32]. Kalita, D. J., & Deka, R(2024). Optimizing Anchoring Groups in D-Π-A Sensitizers for Coumarin-Benzothiazole Based Dsscs: A Dft/Tddft Study. *Tddft Study*. https://dx.doi.org/10.2139/ssrn.5019494

[33]. Choudhary, V., Bhatt, A., Dash, D., & Sharma, N. (2019). DFT calculations on molecular structures, HOMO–LUMO study, reactivity descriptors and spectral analyses of newly synthesized diorganotin (IV) 2-chloridophenylacetohydroxamate complexes. Journal of computational chemistry, 40(27), 2354-2363. https://doi.org/10.1002/jcc.26012

[34]. Bulat, F. A., Murray, J. S., & Politzer, P. (2021). Identifying the most energetic electrons in a molecule: The highest occupied molecular orbital and the average local ionization energy. Computational and Theoretical Chemistry, 1199, 113192. https://doi.org/10.1016/j.comptc.2021.113192

[35]. Nadaf, Y. F., Sushma, G. N., Suma, M., & Sultana, W. (2022). Spectroscopic, Molecular Structure, FMO And Thermodynamic Properties of 11-Chloro-12 (Methylsulfanyl) Quinoxaline Molecule using DFT. Journal of Advanced Scientific Research, 13(04), 51-58. https://doi.org/10.55218/JASR.202213410

[36]. Ramesh, G., & Reddy, B. V. (2023). Investigation of barrier potential, structure (monomer & dimer), chemical reactivity, NLO, MEP, and NPA analysis of pyrrole-2-carboxaldehyde using quantum chemical calculations. Polycyclic Aromatic Compounds, 43(5), 4216-4230. https://doi.org/10.1080/10406638.2022.2086889

[37]. Putz, M. V. (2006). Systematic formulations for electronegativity and hardness and their atomic scales within density functional softness theory. International Journal of Quantum Chemistry, 106(2), 361-389. https://doi.org/10.1002/qua.20787

[38]. Sessa, F., & Rahm, M. (2022). Electronegativity equilibration. The Journal of Physical Chemistry A, 126(32), 5472-5482. https://doi.org/10.1021/acs.jpca.2c03814

[39]. Agwamba, Ernest C., Akaninyene D. Udoikono, Hitler Louis, Esther U. Udoh, Innocent Benjamin, Azuaga T. Igbalagh, Henry O. Edet, Emmanuel U. Ejiofor, and Ugi B. Ushaka. "Synthesis, characterization, DFT studies, and molecular modeling of azo dye derivatives as potential candidate for trypanosomiasis treatment." Chemical Physics Impact 4 (2022): 100076.

[40]. R., Annoji Reddy., Vibha., Prachalith, N. C., Ravikantha, M. N., Shilpa, K. G., & Thipperudrappa, J. (2023). Theoretical and Experimental Investigations of antibiotic agents Sulfamethoxazole (SMX) and Trimethoprim (TMP) by Density Functional Theory. Mapana Journal of Sciences, 22(1). https://doi.org/10.12723/mjs.64.10

[41]. Bhavya, P., Melavanki, R., Sharma, K., Kusanur, R., Patil, N. R., & Thipperudrappa, J. (2019). Exploring the spectral features and quantum chemical computations of a novel biologically active heterocyclic class of compound 2MEFPBA dye: Experimental and theoretical approach. Chemical data collections, 19, 100182. https://doi.org/10.1016/j.cdc.2019.100182

[42]. Prachalith, N. C., Vibha, K., Shilpa, K. G., Ravikantha, M. N., Thipperudrappa, J., & Khadke, U. V. (2023). Quantum computations of non-steroidal anti-inflammatory drug molecules using Density Functional Theory. Chemical Physics Impact, 7, 100317. https://doi.org/10.1016/j.chphi.2023.100317

[43]. Landis, C. R., & Weinhold, F. (2014). The NBO view of chemical bonding. The Chemical Bond: Fundamental Aspects of Chemical Bonding, 91-120. https://doi.org/10.1002/9783527664696.ch3

[44]. Patil, D. S., Avhad, K. C., & Sekar, N. (2018). Linear correlation between DSSC efficiency, intramolecular charge transfer characteristics, and NLO properties–DFT approach. Computational and Theoretical Chemistry, 1138, 75-83. https://doi.org/10.1016/j.comptc.2018.06.006

[45]. Vibha, K., Prachalith, N. C., Reddy, R. A., Ravikantha, M. N., & Thipperudrappa, J. Computational studies on sulfonamide drug molecules by density functional theory. Chemical Physics Impact. https://doi.org/10.1016/j.chphi.2022.100147

[46]. Siddiqui, N., & Javed, S. (2021). Quantum computational, spectroscopic investigations on ampyra (4-aminopyridine) by dft/td-dft with different solvents and molecular docking studies. Journal of Molecular Structure, 1224, 129021. https://doi.org/10.1016/j.molstruc.2020.129021

[47]. Pires, D. E., Blundell, T. L., & Ascher, D. B. (2015). pkCSM: predicting small-molecule pharmacokinetic and toxicity properties using graph-based signatures. Journal of medicinal chemistry, 58(9), 4066-4072. https://doi.org/10.1021/acs.jmedchem.5b00104

[48]. Daina, A., Michielin, O., & Zoete, V. (2017). SwissADME: a free web tool to evaluate pharmacokinetics, drug-likeness and medicinal chemistry friendliness of small molecules. Scientific reports, 7(1), 42717. https://doi.org/10.1038/srep42717

[49]. Farihi, A., Bouhrim, M., Chigr, F., Elbouzidi, A., Bencheikh, N., Zrouri, H., Nasr, F.A., Parvez, M.K., Alahdab, A. and Ahami, A.O.T., 2023. Exploring Medicinal Herbs' Therapeutic Potential and Molecular Docking Analysis for Compounds as Potential Inhibitors of Human Acetylcholinesterase in Alzheimer's Disease Treatment. Medicina, 59(10), p.1812. https://doi.org/10.3390/medicina59101812

[50]. Fathallah, N., El Deeb, M., Rabea, A. A., Almehmady, A. M., Alkharobi, H., Elhady, S. S., & Khalil, N. (2023). Ultra-Performance Liquid Chromatography Coupled with Mass Metabolic Profiling of Ammi majus Roots as Waste Product with Isolation and Assessment of Oral Mucosal Toxicity of Its Psoralen Component Xanthotoxin. *Metabolites*, *13*(10), 1044. https://doi.org/10.3390/metabo13101044

[51]. Islamoğlu, F. (2024). Molecular docking, bioactivity, adme, toxicity risks, and quantum mechanical parameters of some 1, 2-dihydroquinoline derivatives were calculated theoretically for investigation of its use as a pharmaceutical active ingredient in the treatment of multiple sclerosis (MS). Prospects in Pharmaceutical Sciences, 22(4), 168-187. https://doi.org/10.56782/pps.261